HHS Public Access

Author manuscript

Stem Cells. Author manuscript; available in PMC 2017 November 16.

Published in final edited form as:

Stem Cells. 2016 October ; 34(10): 2587–2600. doi:10.1002/stem.2433.

Improved Mobilization of Exogenous Mesenchymal Stem Cells to Bone for Fracture Healing and Sex Difference

Wei Yao[a], **Yu-An Evan Lay**[a], **Alexander Kot**[a], **Ruiwu Liu**[b], **Hongliang Zhang**[a], **Haiyan Chen**[a], **Kit Lam**[b], and **Nancy E. Lane**[a]

[a]Department of Internal Medicine, Center for Musculoskeletal Health, University of California at Davis Medical Center, Sacramento, California, USA

[b]Department of Biochemistry and Molecular Medicine, University of California at Davis Medical Center, Sacramento, California, USA

Abstract

Mesenchymal stem cell (MSC) transplantation has been tested in animal and clinical fracture studies. We have developed a bone-seeking compound, LLP2A-Alendronate (LLP2A-Ale) that augments MSC homing to bone. The purpose of this study was to determine whether treatment with LLP2A-Ale or a combination of LLP2A-Ale and MSCs would accelerate bone healing in a mouse closed fracture model and if the effects are sex dependent. A right mid-femur fracture was induced in two-month-old osterix-mCherry (Osx-mCherry) male and female reporter mice. The mice were subsequently treated with placebo, LLP2A-Ale (500 μg/kg, IV), MSCs derived from wild-type female Osx-mCherry adipose tissue (ADSC, 3×10^5, IV) or ADSC + LLP2A-Ale.

In phosphate buffered saline-treated mice, females had higher systemic and surface-based bone formation than males. However, male mice formed a larger callus and had higher volumetric bone mineral density and bone strength than females. LLP2A-Ale treatment increased exogenous MSC homing to the fracture gaps, enhanced incorporation of these cells into callus formation, and stimulated endochondral bone formation. Additionally, higher engraftment of exogenous MSCs in fracture gaps seemed to contribute to overall fracture healing and improved bone strength. These effects were sex-independent.

There was a sex-difference in the rate of fracture healing. ADSC and LLP2A-Ale combination treatment was superior to on callus formation, which was independent of sex. Increased mobilization of exogenous MSCs to fracture sites accelerated endochondral bone formation and enhanced bone tissue regeneration.

Correspondence: Wei Yao, M.D., Ph.D., Department of Medicine University of California at Davis Medical Center Sacramento, California 95817, USA. Telephone: 916-734-0763; Fax: 916-734-4773; yao@ucdavis.edu.

Author Contributions

W.Y.: Conception and design, collection and assembly of data, data analysis and interpretation, manuscript writing and final approval of manuscript. E.A.Y., R.W.L., H.L.Z., and H.L.C.: Collection and assembly of data, data analysis and interpretation, and final approval of manuscript. A.K.: Collection and assembly of data, data analysis and interpretation, manuscript writing and final approval of manuscript. K.L. and N.E.L.: Conception and design, data analysis and interpretation, and final approval of manuscript.

Disclosure of Potential Conflicts of Interest

The authors indicate no potential conflicts of interest.

Keywords

Bone-targeted; Adipose-derived stromal cells; Angiogenesis Osteogenesis; Fracture healing

Introduction

Traumatic fractures during an individual's lifetime often require hospitalization, surgery, frequent physician visits and lost time from work. More than 5 million Americans suffer from fractures annually. In 2010, falls among older adults cost the U.S. health care system $30 billion and by 2020, the annual direct medical costs will total $68 billion (Quoted from the Centers for Disease Control and Prevention). The morbidity associated with fracture healing is high and there is currently no approved medical therapy to accelerate fracture healing in long bones. The efficacy of parathyroid hormone (PTH) in fracture healing has been evaluated in rodents [1–3] and, although not approved through the FDA for this indication, recombinant human PTH fragment 1–34 has been used off-label in clinical practice [4–6]. Local infusions with recombinant human bone morphogenetic protein (rhBMP) 2 and 7 have been used to treat open tibial shaft fractures and long bone non-unions although the efficacy of these treatments remains controversial [7–13]. Several side effects have been associated with the rhBMPs such as ectopic bone formation, tumorigenesis and the development of antibodies against rhBMPs [10, 14–17]. Currently, there is still an unmet medical need for accelerating fracture healing.

The activation and migration of endogenous mesenchymal stromal cells (MSCs) are critical for fracture healing [18]. MSCs can differentiate into osteoblasts and chondroblasts, where cartilage serves as a building block for additional bone formation, thereby bridging fracture gaps through endochondral ossification [19]. Exogenous MSC transplantation has been tested in animal models and human fractures [20]. It is not known whether these transplanted MSCs directly home to fracture sites and participate in the healing process or indirectly influence healing by acting as "secretory machines" of growth factors and inflammatory cytokines [21–27]. We have developed a bone-seeking compound, LLP2A-Alendronate (LLP2A-Ale) that selectively targets the integrin $\alpha 4\beta 1$ on the cell surface. We have previously shown that LLP2A-Ale has a high affinity for MSCs and increased MSC migration and differentiation into osteoblasts in vitro, especially in the presence of hydroxyapatite. Most importantly, LLP2A-Ale increased exogenous MSC homing to bone and reversed bone loss in mouse models of aging and estrogen-deficiency [28, 29]. One of the goals of our current report was to evaluate the effect of bone-target delivery of MSC therapy on fracture healing during injury and tissue repair.

Sex differences are common in skeletal tissue [30]. Before menopause, stress fractures are more common in females than in their male counterparts [31]. Donor cell and host sex significantly affect the healing process [32–36]. MSCs derived from bone marrow obtained from young male mice have higher doubling times than that of their aged-matched female-derived counterparts [35]. Muscle-derived stem cells (MDSCs) obtained from male donors displayed more osteogenic and chondrogenic potential than those obtained from female donors [37, 38], but female-derived MDSCs had higher muscle regeneration efficacy than

male-derived cells [33, 39, 40]. Host sex also significantly affects the regenerative capacity of MSCs [32, 34]. Unfortunately, except for a single study [34], a majority of the current peer-reviewed publications concerning the use of MSCs for fracture repair did not specify the donor sex of the transplanted cells [41–45]. A goal of the study was to evaluate if there were intrinsic sex differences influence fracture healing. A second goal of this study was to determine the treatment efficacy with MSCs, LLP2A-Ale or a combination of both in a closed fracture model.

Materials and Methods

Mouse Strains and Animal Procedures

We took advantage of reporter mouse lines to visualize both the MSC engraftment and endogenous osteogenesis during fracture repair. Reporter mice were obtained via MTA agreement from Dr. Peter Maye at the University of Connecticut Health Center. Closed transverse diaphyseal fractures of the right femur were generated in 2-month-old mice using a previously described method with some modification [46, 47]. Briefly, a 0.38-mm-diameter stainless-steel pin was inserted into the medullary canal. Fractures were created at the midfemur using a drop-weight blunt guillotine device. Success of the fractures and pin placement were confirmed by x-ray (Faxitron, Lincolnshire, IL). Mice with fractures of both sexes were treated with placebo (phosphate buffered saline, PBS), LLP2A-Ale (500 μg/kg, IV at day 1) or adipose-derived MSCs (ADSCs) obtained from WT mice transduced to express green-florescence protein-vector (GFP) (ADSC-GFP, 3×10^5, IV in the tail vein at day 1) with or without LLP2A-Ale. Mice were euthanized on days 14, 21 or 42 postfracture. Additional groups from both sexes were treated with rhPTH (1–34) at 25 μg/kg, 5x/week, and euthanized at days 21 and 42 (n = 8–16/ group for both sexes). Mice from the day 42 group received subcutaneous injections of calcein (10 mg/kg) seven and two days before being killed on day 42.

A separate set of experiments was performed using male Col12.3kb-GFP mice as recipients of ADSCs obtained from female Osx-mCherry mice. Col12.3kb-GFP mice had marked endogenous osteogenesis and Osx-mCherry mice had marked endogenous osteoprogenitor cells, including chondrocytes and osteoblasts that participate in both endochondral and intramembranous bone formation during fracture healing [48–50]. The Col12.3kb-GFP mice were euthanized at day 7 postfracture (N = 3/group). The Institutional Animal Care and Use Committee at UC Davis approved all animal procedures.

ADSC Isolation and Culture

Adipose tissue was collected from the abdominal and inguinal regions, incubated with 0.1% type I collagenase solution in a 195-rpm shaker at 37°C for 90 minutes, centrifuged at 300 g for 5 minutes, shaken vigorously for 15 seconds and centrifuged at 300 g for an additional 5 minutes at room temperature. The dark cell pellets were collected, suspended in PBS containing 10% BSA and centrifuged at 300 g for 5 minutes. The cell pellets were then suspended in cold 1× Magcellect plus via a negative selection principle (CD45-, TER119-; EasySep Mouse Mesenchymal Stem/Progenitor Cell Enrichment Kit, Stem cell Technologies, Vancouver, Canada). The cells were maintained in Mesencult mouse MSC

proliferation medium (Stem cell Technologies Inc., Vancouver, BC, Canada) and used at passage 2. These cells were 99.99% CD45 negative and positive for CD105 (>70%), CD29 (>99%), and Sca1 (>98%).

MicroCT Measurement for the Callus

The microCT protocol was modified to reflect the variation in mineralization during fracture [51]. Briefly, the right distal femurs were scanned by μCT (VivaCT 40, Scanco Medical AG, Bassersdorf, Switzerland) at 55 KeV and 145 μA at an isotropic resolution of 10.5 μm in all three dimensions, with an integration time of 350 ms. The entire callus was scanned. The outer boundary of the callus was manually defined by contouring every 4 mm, covering the full length of the callus. Gaussian filtering with sigma 1.2 and support 2 were used to minimize the image noise. We used different thresholds to separate new bone and calcified cartilage (250–350) from well-mineralized cortical bone (350–800). The same settings and thresholds were used for all samples [28, 29, 52, 53]. Data for new bone callus are presented, including total callus volume (TV), callus new bone volume (CV), callus volume fraction (CV/TV) and volumetric bone mineral density (vBMD).

Real-Time RT-PCR

Total RNA was isolated from the fracture callus at day 14 using a modified two-step purification protocol employing homogenization (PRO250 Homogenizer, 10 mm × 105 mm generator, PRO Scientific IN, Oxford CT) in Trizol (Invitrogen, Carlsbad, CA), followed by purification over a Qiagen RNeasy column (Qiagen, Valencia, CA). RT-PCR gene pathway arrays focused on wound healing were purchased from SABiosciences (Frederick, MD) and included genes in the following categories: ECM Components (COL14A1, COL1A1, COL1A2, COL3A1, COL4A1, COL4A3, COL5A1, COL5A2, COL5A3, VTN), Remodeling Enzymes (Ctsg, Ctsk, Ctsl, F13a1, F3 (Tissue Factor), Fga (Fibrinogen), Mmp1a, Mmp2, Mmp7, Mmp9, Plat (tPA), Plau (uPA), Plaur (uPAR), Plg (plasminogen), Serpine1 (PAI-1 [Plasminogen activator inhibitor 1]), Timp1), Cellular Adhesion (Cdh1 (E-cadherin), Itga1, Itga2, Itga3, Itga4, Itga5, Itga6, Itgav, Itgb1, Itgb3, Itgb5, Itgb6), Cytoskeleton (Acta2 (a-SMA), Actc1, Rac1, Rhoa, Tagln), Inflammatory Cytokines & Chemokines (Ccl12, Ccl7 (Mcp-3), Cd40lg (Tnfsf5), Cxcl1, Cxcl11 (I-TAC/IP-9), Cxcl3, Cxcl5 (ENA-78/LIX), Ifng, Il10, Il1B, Il2, Il4, Il6) and Growth Factors (Angpt1, Csf2 (GM-CSF), Csf3 (GCSF), Ctgf, Egf, Fgf10, Fgf2, Fgf7, Hbegf (Dtr), Hgf, Igf1, Mif, Pdgfa, Tgfa, Tgfb1, Tnf, Vegfa). Data are presented as fold-differences from the placebo-treated (PBS) group for both sexes.

Immunohistochemistry

Immunohistochemical staining was performed on frozen callus sections using anti-mouse rabbit αSMA and CD31 antibodies (1:200 and 1:50 dilution, respectively, Abcam, Cambridge, MA). The secondary antibody was Alexa-Fluor 350-conjugated goat anti-rabbit IgG (1:1,000, Vector laboratories Burlingame, CA). Forty, 6-diamino-2-phenylindole (DAPI) solution (1:5,000, Vector laboratories) was applied for 5 minutes for nuclear staining.

Serum Bone Marker and Cytokines/Chemokines Measurement

Serum levels of osteocalcin and CTX-1 were measured by ELISA (Biomedical Technologies, Stoughton, MA) and cytokines/chemokines profiles were measured by multiplexing (EMD Millipore, Billerica, MA). All measurements were performed in duplicate for each sample following the manufacturer's instructions. Cytokines/chemokines with significant changes between the treatment groups and the placebo-treated (PBS) group are presented in Supporting Information Figure 2.

LLP2A-Ale Bone Affinity Experiments

To evaluate the affinity of LLP2A-Ale for bone, we first conjugated alendronate or LLP2A-Ale to biotin at 4:1 molar. A fluorescent, streptavidin - Alexa Fluor 488 (SA-Alexa488) that had high affinity for biotin, was used as a secondary detection reagent for histochemical application in vivo. Alendronate-biotin was mixed with SA-Alexa488 at 4:1 molar before it was injected intravenously at 100 μl/mouse. The mice were sacrificed 8 hours after the injection. The femurs were embedded in methyl methacrylate and cut into 30 μm-thick sections.

As part of an IND enabling study for the FDA, a vendor (Covance Laboratories, Madison, WI) performed the following study to track the affinity of LLP2A-Ale for bone and its tissue distribution over time. To track the affinity of LLP2A-Ale to bone and its tissue distribution overtime, radiolabeled LLP2A-Ale was prepared by incorporation of ^{14}C into the alendronate portion of the molecule. ^{14}C-LLP2A-Ale in water vehicle was injected intravenously into male Harlan Sprague Dawley rats (205–231 g; 7 weeks of age), at a dose of 1 mg/kg. Rats were then euthanized at 24, 48, 72, 96, 120, and 168 hours post-injection (n = 5 rat per time point). Animals were exsanguinated and carcasses were collected for quantitative whole-body autoradiography. The carcasses were immediately frozen in a hexane/dry ice bath for approximately 8 minutes and stored at approximately –70°C for at least 2 hours. The frozen carcasses were embedded in chilled carboxymethylcellulose and frozen into blocks. Standards fortified with ^{14}C radioactivity were placed into the frozen block for monitoring the uniformity of section thickness. Sections were collected on adhesive tape at 40 μm thickness, in a Leica CM 3600, at five levels in the sagittal plane. Sections were dried, then wrapped with Mylar film and exposed on phosphor-imaging screens along with fortified blood standards for subsequent calibration of the image analysis software. Screens were exposed for four days. Exposed screens were scanned using a Storm scanner. The autoradiographic standard image data were sampled using InterFocus Imaging Ltd. MCID™ Analysis software was used to create a calibrated standard curve.

Histology

Whole femurs were dissected and intramedullary pins were removed. The femurs were fixed in 10% formalin for one day at 4°C before scanning by microCT. Femurs with calluses were then soaked in 30% sucrose in PBS at 4°C for eight hours and then embedded in Tissue-Tek O.C.T. (Sakura Finetek USA, Inc., Torrance, CA). Longitudinal sections through the entire callus were obtained with a Leica microtome (Leica, Wetzlar, Germany) and Cryofilm (Section lab, Hiroshima, Japan). The slides were mounted with 50% glycerol in PBS. Imaging was performed on a Keyence BZ-X700 all-in-one Fluorescence Microscope (Itasca,

IL). Osx+ or GFP+ area were measured using Keyence cell count software and were normalized by total callus area. Bone histomorphometry was performed on the entire callus, in which total bone surface, single labeled and doubled labeled surface were measured with a semiautomatic image analysis system (Bioquant Image Analysis Corp., Nashville, TN) [52–55]. Mineralized surface (MS/BS) and bone formation rate (BFR/BS) were calculated [55, 56]. Bone histomorphometric terminology was consistent with recommendations of the American Society for Bone and Mineral Research [55]. We have reported similar methodology in previous experiments in our laboratory [57–60].

Bone Strength Measurements

Each femur was loaded to failure along its long axis using an MTS 831 electro-servo-hydraulic testing system (MTS Systems Corp., Eden Prairie, MN) at a displacement rate of 0.01 mm/s with a 90 N load cell. Sample loads and displacements were continuously recorded throughout each test. Maximum load was determined from the load-displacement curve and the work to fracture was calculated from the area under the load-displacement curve [28, 52, 53, 61].

Statistical Analyses

The group means and standard deviations (SDs) were calculated for all outcome variables. Nonparametric *Kruskal-Wallis* and Tamhane Post Hoc tests were used to determine differences between treatment and placebo groups for the same sex. RT-PCR data are presented as fold-changes from the PBS-treated group. Two factor ANOVA was used to evaluate treatment and sex effect and their interactions for each individual parameter within a same treatment. Un-paired t-tests were used to compare real time RT-PCR or multiplexing data from the treatment group with the PBS-treated group. Linear regression was performed between callus structural parameters and bone strength parameters. Differences were considered significant at $p < .05$ (GraphPad Prism 6, La Jolla, CA).

Results

Affinity of LLP2A-Ale for Bone

Mice that received SA-Alexa488 (100 μl/mouse) alone did not show green fluorochrome labeling at bone surfaces (data on file). In comparison, mice that received alendronate conjugated to biotin and SA-Alexa488 had green fluorescence predominantly at the periosteal surface of the mid-femoral shaft (arrows). When alendronate was conjugated to LLP2A, green fluorochrome labeling was observed at the periosteal and endocortical surfaces, and within canaliculi (Supporting Information Fig. 1A).

LLP2A-Ale$^{C\text{-}14}$ was deposited in skeletal tissues (humerus, tibia, femur, and rib) as well as in the kidney during the first 24-hours, peaking at 48–72 hours. The percent of the radioactive dose that ended up in the bone at 24, 48, 72, 96, 120, and 168 hours was 37, 36, 34, 29, 27, and 29 %, respectively (Supporting Information Fig. 1B).

Engraftment of Transplanted Cells in the Fracture Callus and Treatment Effects on Endogenous Osteogenesis

To visualize the early engraftment of MSCs in bone with or without LLP2A-Ale, we gave male Col12.3kb-GFP mice, which had marked endogenous bone formation, ADSCs obtained from female Osx-mCherry mice. We found that LLP2A-Ale significantly increased the engraftment of the Osx+ in the callus (1.76%; white arrows, Supporting Information Fig. 2) and was associated with a 48% increase in GFP+ cell populations as compared to the PBS-treated group (14 ± 2% in PBS and 20% in LLP2A-Ale +/− ADSC; $p < .05$; Supporting Information Fig. 2).

Osx-mCherry reporter mice were used as fracture hosts and euthanized at day 14, 21, or 42. ADSCs derived from WT littermates were transduced to express GFP and given to the Osx-mCherry mice. We observed sparse GFP+ transplanted cells within the fracture gaps in the ADSC only groups at day 14 (4.0 ± 1.2%; Fig. 1B). Some transplanted cells were found to have migrated to the fracture gaps in the ADSC + LLP2A-Ale groups (9.2 ± 1.4%; $p < .05$ vs. ADSC) and some transplanted cells were incorporated in the callus, participating in endochondral bone formation (Fig. 1C, 1D, white arrows; Fig. 3D, green arrows). The transplanted cells were also located in areas adjacent to dead bone fragments (Fig. 1E). At day 21, GFP+ transplanted cells were sparsely detected (< 1%) in the bone marrow within the central regions of the callus in all groups that received ADSCs (Fig. 2A, white arrow heads). In the ADSC + LLP2A-Ale cotreatment group, some of these GFP+ cells were seen within bone marrow (Fig. 2B), bridging the fracture gap, condensing to form bony islands (Fig. 2C, yellow arrow heads), incorporating into the callus mineralization front or embedding within the callus (3 ± 0.7%, $p < .05$ vs. ADSC) (Fig. 2C, yellow arrow heads). We examined potential mineralization in the right hindlimb muscles using microCT and frozen sections and did not detect ossification. Transplanted cells were not detected in other tissues as measured using qPCR by day 21 (data on file). These results suggest that some ADSCs migrate to fracture gaps and differentiate into osteoblasts or osteocytes, while very few of them remain in bone marrow within the callus for up to 21 days.

Endogenous bone formation was measured by the activation of osterix + (OSX+) cells. In female recipients, the OSX+ cell density was increased by approximately 50% in the LLP2A-Ale and ADSC + LLP2A-Ale cotreatment group at day 14 ($p < .05$ vs. PBS). At day 21 the LLP2A-Ale, ADSC + LLP2A-Ale cotreatment and PTH groups had significantly higher OSX+ cell density ($p < .05$ vs. PBS). In male recipients, the ADSC + LLP2A-Ale cotreatment group had 30% higher OSX+ density at day 14 ($p < .05$ vs. PBS). By day 21, the OSX+ density was similar among the male treatment groups (Fig. 3, Supporting Information Figure 3).

Effects of ADSCs with or without LLP2A-Ale on Early Wound-Healing Responses

We examined the wound-healing response at the fracture site 14 days post-fracture, representing the transition from the inflammation/hematoma formation phase to the MSC recruitment and bone formation phase. There were no changes among treatment groups in the mRNA levels of ECM components, cellular adhesion, including integrin α4 and β1 subunits. Compared to the placebo groups, mRNA expression of remodeling enzymes,

namely Fga and Plg, was increased in the ADSC + LLP2A-Ale cotreatment groups, while MMP7 expression was decreased in the LLP2A-Ale only groups. Inflammatory cytokine/chemokine gene expression, including Cxcl3, INF-γ, IL-6, and IL-10, was increased by 1.5–2.5-fold in the ADSC + LLP2A-Ale cotreatment groups compared with the placebo groups, especially for the females. Acta2, the gene encoding the alpha smooth muscle actin (α-SMA), was increased in the LLP2A-Ale only groups and the ADSC + LLP2A-Ale cotreatment groups (Fig. 4A, 4B). α-SMA expression was reported to arise primarily from the periosteum [62, 63] and contributed to callus formation during fracture healing. In agreement with our RT-PCR results, we found that α-SMA expression at the periosteal surface was very low in the placebo and ADSC only groups but was increased to detectable levels in the LLP2A-Ale only groups and was significantly increased in the ADSC + LLP2A-Ale cotreatment groups (Fig. 4D, white arrows, green fluorescent cells). Some of these α-SMA+ cells coexpressed osterix (Fig. 3D, yellow arrows, yellow fluorescent cells), suggesting that they differentiated along an osteoblastic lineage and improved callus formation. The expression of growth factors and angiogenesis genes, including Egf, Fgf2, Hbegf, Hgf and Vegfa, was suppressed by ADSC monotherapy in the males ($p < .05$ vs. PBS). These genes were increased by 1.4–2.5-fold ($p < .05$ vs. PBS) in the ADSC + LLP2A-Ale cotreatment groups compared with the PBS-treated groups, especially in the females. Blood vessel formation, as shown by anti-CD31 staining, was detected more frequently in the ADSC+ LLP2A-Ale cotreatment groups than in the other groups (Fig. 4E).

Effects of ADSCs with or Without LLP2A-Ale on Systemic Inflammation

Cytokine/chemokine profiling was performed on serum samples collected at days 14, 21, and 42 to monitor systemic inflammatory responses following fracture and treatment. Most of the cytokines/chemokines were not detectable in the serum but some, including G-CSF, LIX, Ip-10, K.C., M-CSF, and MIP-2, were detectable although their levels did not change with the different treatments. ADSC treatment significantly increased IL-13, MCP-1/CCL2, and MCP_2/CXCL2 levels ($p < .05$ vs. PBS) for both sexes (Supporting Information Fig. 4). In female mice, LLP2A-Ale treatment decreased IL-1α at days 14–21 and returned to PBS-control levels by day 42. In male mice, IL-α levels were lower than in the PBS-control group in both the LLP2A-Ale and ADSC+ LLP2A-Ale cotreatment groups from days 7 to 42 (Supporting Information Fig. 4).

Effects of ADSCs with or Without LLP2A-Ale on Callus Formation

At day 21, PTH treatment induced the largest TV in both males and females. However, callus mineralization mainly occurred along the fractured ends, very little mineralized tissue was detected within the fracture gaps, and there was a lack of new bone formation bridging the fractures. CV/TV and callus vBMD did not differ compared with the placebo groups. LLP2A-Ale only, ADSC only and the cotreatment tended to increase the CV/TV and callus vBMD compared with the day 21 female placebo group. Male ADSC + LLP2A-Ale cotreated mice had increased callus vBMD compared with the placebo group at day 21 ($p < .05$; Supporting Information Fig. 5).

At day 42, the female ADSC + LLP2A-Ale cotreatment group had a higher CV/TV and callus vBMD compared with the placebo group ($p < .05$). The male LLP2A-Ale only and

ADSC + LLP2A-Ale cotreatment groups had a higher CV/TV and callus vBMD compared with the placebo group ($p < .05$; Fig. 5).

None of the treatments significantly affected serum CTX1, a bone resorption marker, as compared to PBS controls (Fig. 6). Systemic bone formation, as measured by serum osteocalcin levels at day 42, was similar among all treatment groups, except for PTH-treated males ($p < .05$ vs. PBS; Fig. 6). Callus bone formation and remodeling of the callus were measured by bone histomorphometry. The surface-based bone formation rate was significantly higher in the ADSC + LLP2A-Ale cotreatment group in both female and male recipient mice ($p < .05$ vs. PBS), with increased double-labeled callus surface and inter-label distance ($p < .05$ vs. PBS; white arrows), indicating active mineral apposition following the combination treatment (Fig. 6A, 6B).

Effects of ADSC with or Without LLP2A-Ale on Bone Strength

Mechanical testing is the ultimate method to determine an intervention's effect on fracture healing. Maximum load, which reflects the general integrity of bone structure [64], was increased in the female PTH-treated group and both ADSC + LLP2A-Ale cotreatment groups ($p < .05$ vs. PBS). Work-to-failure (area under the load-displacement curve), the amount of energy necessary to break the bone, was higher in the female LLP2A-Ale treated group and both ADSC + LLP2A-Ale cotreatment groups ($p < .05$ vs. PBS; Fig. 7A).

To determine whether callus mass, structure and geometry affected bone strength and if this differed according to sex, we performed a linear regression between the structural parameters obtained from microCT measurements (TV, CV, CV/TV and vBMD) and biomechanical parameters (maximum load and work-to-failure). We found that the main determinants for maximum load were CV/TV and callus vBMD for both females and males (Fig. 7B). In females only, the main determinants for work-to-failure were TV and callus vBMD (Fig. 7C).

Discussion

Our data indicate that engraftment efficacy can be increased using the "bone-targeting" agent LLP2A-Ale, which improves the homing of transplanted ADSCs to the fracture callus. These cells were initially observed around the dead bone fragments, within fracture gaps, and participated in endochondral bone formation to form callus bridges. Although we observed some changes in the systemic cytokine and chemokine levels, these changes seemed to have resulted from fracture and not from our interventions. Most importantly, the cotreatment of ADSC and LLP2A-Ale resulted in higher callus volume fraction, higher mineralization of the callus and higher bone strength (work-to-failure) compared with the placebo group.

Sex-differences were observed in the therapeutic effects of LLP2A-Ale monotherapy and cotreatment with ADSCs. In female recipients, cotreatment was superior to LLP2A-Ale monotherapy for callus bone formation, mineralization and bone strength. In male recipients, cotreatment had similar effects on callus formation and callus mineralization compared to the LLP2A-Ale monotherapy. However, the bone strength was higher only in

the cotreatment group, suggesting an intrinsic improvement in callus material properties following cotreatment.

The application of MSCs for bone regeneration has focused primarily on increasing the number of bone-forming progenitor cells in the fracture callus to directly augment bone formation. Both autologous and allogeneic stem cells transplantations have been somewhat successful for wound repair [42, 65, 66]. We found that ADSC transplantation by itself led to very few cells homing to the fracture gaps or participating in callus formation. In contrast, directed to the fracture site was greatly increased by cotreatment with the bone-targeted compound LLP2A-Ale. These exogenous cells were initially observed to surround dead bone fragments, presumably due to alendronate's affinity for hydroxyapatite, as well as possibly due to death signals released by these bone fragments attracting the migration of MSCs [67] (Fig. 1C, 1E). At days 14 and 21, most of the exogenous MSCs were found within the center of the fracture gaps (Fig. 2A, 2B). Some of the exogenous cells (GFP+) were seen incorporated into the callus and embedded in the mineralization front, forming bone-like foci (Fig. 2C) and bridging the fracture gaps. We did not observe any transplanted cells engrafted at the periosteal surface. α-SMA+ cells were found to arise from the periosteum and contribute to fracture healing. We did observe more α-SMA+ cells (Fig. 4D, green cells, white arrows) especially in the ADSC + LLP2A-Ale-treated groups. Some of these cells differentiated into osteoblasts that were positive for both α-SMA and osterix (Fig. 4D, yellow cells, yellow arrows). Because α-SMA-CreERT mice were not available to us at the time these studies were performed, we were unable to trace the populations of these cells prior to fracture and after treatment. Collectively, these findings support our contention that LLP2A-Ale treatment increases homing of transplanted cells to fracture gaps, and that these exogenous cells directly contribute to endochondral bone formation.

Recently, the focus for MSC transplantation has shifted from a cell replacement method for osteogenesis to the paracrine effects of MSCs, including their potential secretion of growth factors such as PDGF, FGF or VEGF, which may in turn either increase osteoprogenitor cells or increase vascularization. Callus tissue expresses high levels of vascular inhibitory molecules such as thrombospondins (TSPs), which block angiogenesis. The destruction of TSPs with a TSP2 knock-out mouse model resulted in reduced endochondral ossification and enhanced appositional bone formation [68, 69]. The Plg system is the primary fibrinolytic pathway responsible for clot dissolution after thrombosis [70]. PAI-1 is consistently unregulated in ischemic conditions in vitro, and PAI-1 is a negative regulator of MSC survival in vivo [71]. At day 14, we found that Plg was among the most significantly upregulated genes, especially in the cotreatment group, suggesting this therapy may accelerate clot dissolution and enhance angiogenesis. Fga, an ECM protein that enhances MSC proliferation [72] and supports MSC differentiation into osteoblasts [73], was also significantly upregulated following cotreatment. Matrix metalloproteinases 7 and 9 (MMP7, MMP9), whose temporal expression pattern correlates with chondrogenesis [74, 75], were downregulated following LLP2A-Ale with or without ADSC cotreatment. This suggests that the acceleration of endochondral bone formation and remodeling corresponded to increased bone mineralization rate and bone formation at day 42. Taken together, our data suggest that synergistic angiogenic effects with ADSCs and LLP2A-Ale during the early phase of fracture repair.

Inflammatory responses are essential for bone healing. One of the primary roles of inflammation is to clear cellular debris. Some of the immunomodulatory effects of MSCs rely on cell-cell contacts between MSCs and immune cells. For example, direct MSC contact with CD4+ cells required to induce CD4 + CD25 + FoxP3+ Treg cells, which was followed by increased expression of TGF-β1 and PGE2 [76]. When MSCs were exposed to pro-inflammatory cytokines such as IFNγ and TNFα, they became activated and modulated IL-10 production by B cells through a contact-dependent mechanism [77, 78]. IFNγ was required to initiate MSC efficacy [79] and is known to enhance the immunosuppressive properties of MSCs [80]. "Licensed" MSCs modulate the phenotypic shift of macrophages from the M1 pro-inflammatory type to the M2 anti-inflammatory type, thereby promoting the reparative stage of wound healing by secreting anti-inflammatory factors such as IL-10 and IL-6 [81–83]. Allogeneic MSCs have been well-defined by their ability to suppress immune responses in addition to eliciting a weak allogeneic immune response [84]. The MSCs that we used were obtained from adipose tissue from wild-type littermates. We chose to use ADSCs instead of bone marrow-derived MSCs for this study since we found that less than 10% of the cell population from bone marrow were MSCs, as defined by CD45-CD105 + CD29 + Sca1+. On the other hand, the ADSC had very little hematopoietic "contamination" with CD45-cells (>99.99%), which may minimize the potential immunogenicity following allogeneic transplantation. Although our study was not designed to dissect macrophage phenotype or stage-dependent cytokine production in vivo, we observed higher numbers of MSCs engrafted in the fracture callus upon cotreatment with LLP2A-Ale and ADSCs. Cell-cell contact between MSCs and local inflammatory cells, significantly lowered systemic IL-1α levels, and this action may contribute to the immunomodulatory effects in situ at the injury sites. On the other hand, we found higher levels of soluble factors in the circulation in the treatment groups compared with the non-treated animals with fractures, suggesting MSCs may also induce systemic actions. In particular, we found that monocyte chemoattractant proteins MCP-1 and MCP-2 were higher in the ADSC groups, which may support the migration of lymphocytes following allograft ADSC. IL-13 may aid in the balance of M1 to M2 macrophages following allogeneic MSCs [83, 85, 86].

The most critical test of fracture healing is to determine if these interventions restore bone strength. ADSC + LLP2A-Ale cotreatment increased callus bone strength, with more callus volume and denser bone resulting in higher callus mineralization and bone formation. This effect differed somewhat from those induced by PTH or sclerostin-antibody. PTH added new bone to the two fractured ends and did not initially bridge the fracture gap. PTH, when administered at twice the dose used in our current study (25 μg/kg), was reported to act through periosteal progenitor cells and therefore stabilize long bone fractures, inducing higher bone strength compared with non-treated animals, especially in young mice [3]. PTH and MSC cotherapy synergistically increased new bone formation in a rat vertebral defect model as PTH enhanced MSC migration to the lumbar region [87]. Sclerostin-antibody increased callus size and volume and seemed to have an early effect on stabilizing the callus similar to what we observed for ADSC + LLP2A-Ale [88]. ADSCs, when used in combination with LLP2A-Ale, mobilized to the fracture gaps and increased bone mineralization, bridging the fracture gaps as shown at the tissue levels as well as by

microCT. Bridging is generally considered one of the most critical outcomes for fracture healing as it reestablishes the fractured union and is correlated with recovery of bone strength. We observed greater maximum load and work-to-failure at day 42 in the ADSC + LLP2A-Ale groups for both sexes, indicating better extrinsic bone strength. The fraction of callus bone volume and the vBMD of the callus, but not the callus size, were the main determinants for peak bone load in both sexes, suggesting that higher bone strength was associated with improvements in bone mineralized content and bone density. This observation was sex-independent. In females only, the size of the callus contributed to the overall work-to-failure. This suggested that other factors, including intrinsic elements such as collagen content and orientation, tissue age and toughness [19] might play a role in determining overall bone strength, especially for the males in our study.

There is a concern that alendronate may delay fracture healing [89]. It was shown that alendronate treatment at 2 mg/kg/day for 9 weeks delayed fracture healing in beagles [90] and incadronate treatment at 100 μg/kg, 3×/week for 2 weeks caused a delay of cortical bone formation in rats [91]. In our study, alendronate was used as a bone-targeted delivery agent in a conjugated compound (LLP2A-Ale) to increase homing of endogenous or transplanted stem cells to bone as alendronate has very high affinity for hydroxyapatite. The single alendronate dose we used as a "carrier" was approximately 125 ug/kg (3.75 ug/mouse), which was at least tenfold lower that the therapeutic dose for the treatment of osteoporosis (70 mg once weekly or 10 mg daily in humans for up to 5 years, equivalent to approximately 5–25 ug/kg/day in mice). We have never found antiresorptive effects when using similar doses of LLP2A-Ale in mouse models of aging, estrogen-deficiency osteoporosis [28, 29] and glucocorticoid-induced osteoporosis, as well as in rats (data on file).

In conclusion, the bone-targeted delivery of MSCs to the fracture site contributed directly to callus formation via direct bone homing and the differentiation of exogenous MSCs to osteoblasts. Increased engraftment of the exogenous MSCs in the fracture gaps seemed to alter the tissue microenvironment via paracrine signaling through the secretion of chemokines, as well as angiogenic and anti-inflammatory factors that may have contributed to overall fracture healing and improvement in bone strength. The increased mobilization of exogenous MSCs to fracture sites augmented fracture repair through endochondral bone formation, as well as through paracrine signaling, to enhance overall bone tissue regeneration.

Supplementary Material

Refer to Web version on PubMed Central for supplementary material.

Acknowledgments

This work was funded by NIH grant R01 AR061366 (to WY) and California Institute of Regenerative Medicine CIRM-DR2A-05302 (to NEL and WY) and P50 AR063043 (to NEL). We thank Chrisoula Toupadakis, Dr. Clare Yellowley and Dr. Ralph Macucio for their assistance in implementing fracture protocols and technical support, Randall Press and Irina Reynolds at Covance Laboratories, Madison, WI for their contributions in the radiolabeled distribution study.

References

1. Kaback LA, Soung do Y, Naik A, et al. Teriparatide (1–34 human PTH) regulation of osterix during fracture repair. J Cell Biochem. 2008; 105:219–226. [PubMed: 18494002]
2. Alkhiary YM, Gerstenfeld LC, Krall E, et al. Enhancement of experimental fracture-healing by systemic administration of recombinant human parathyroid hormone (PTH 1–34). J Bone Joint Surg Am. 2005; 87:731–741. [PubMed: 15805200]
3. Yukata K, Xie C, Li TF, et al. Aging periosteal progenitor cells have reduced regenerative responsiveness to bone injury and to the anabolic actions of PTH 1–34 treatment. Bone. 2014; 62:79–89. [PubMed: 24530870]
4. Zhang D, Potty A, Vyas P, et al. The role of recombinant PTH in human fracture healing: A systematic review. J Orthop Trauma. 2014; 28:57–62. [PubMed: 23454854]
5. Nakamura T, Sugimoto T, Nakano T, et al. Randomized teriparatide [human parathyroid hormone (PTH) 1–34] Once-weekly efficacy research (TOWER) trial for examining the reduction in new vertebral fractures in subjects with primary osteoporosis and high fracture risk. J Clin Endocrinol Metab. 2012; 97:3097–3106. [PubMed: 22723322]
6. Cipriano CA, Issack PS, Shindle L, et al. Recent advances toward the clinical application of PTH (1–34) in fracture healing. HSS J. 2009; 5:149–153. [PubMed: 19290582]
7. Lee FY, Storer S, Hazan EJ, et al. Repair of bone allograft fracture using bone morphogenetic protein-2. Clin Orthop Relat Res. 2002:119–126.
8. Govender S, Csimma C, Genant HK, et al. Recombinant human bone morphogenetic protein-2 for treatment of open tibial fractures: A prospective, controlled, randomized study of four hundred and fifty patients. J Bone Joint Surg Am. 2002; 84-A:2123–2134. [PubMed: 12473698]
9. Calori GM, Tagliabue L, Gala L, et al. Application of rhBMP-7 and platelet-rich plasma in the treatment of long bone non-unions: A prospective randomised clinical study on 120 patients. Injury. 2008; 39:1391–1402. [PubMed: 19027898]
10. Katayama Y, Matsuyama Y, Yoshihara H, et al. Clinical and radiographic outcomes of posterolateral lumbar spine fusion in humans using recombinant human bone morphogenetic protein-2: An average five-year follow-up study. International Orthopaedics. 2009; 33:1061–1067. [PubMed: 18581064]
11. Jones AL, Bucholz RW, Bosse MJ, et al. Recombinant human BMP-2 and allograft compared with autogenous bone graft for reconstruction of diaphyseal tibial fractures with cortical defects. A randomized, controlled trial. J Bone Joint Surg Am. 2006; 88:1431–1441. [PubMed: 16818967]
12. Friedlaender GE, Perry CR, Cole JD, et al. Osteogenic protein-1 (bone morphogenetic protein-7) in the treatment of tibial nonunions. J Bone Joint Surg Am. 2001; 83-A:S151–S158.
13. White AP, Vaccaro AR, Hall JA, et al. Clinical applications of BMP-7/OP-1 in fractures, nonunions and spinal fusion. Int Orthop. 2007; 31:735–741. [PubMed: 17962946]
14. Yilgor P, Hasirci N, Hasirci V. Sequential BMP-2/BMP-7 delivery from polyester nano-capsules. J Biomed Mater Res A. 2010; 93:528–536. [PubMed: 19585564]
15. Mines D, Gu Y, Kou TD, et al. Recombinant human bone morphogenetic protein-2 and pancreatic cancer: A retrospective cohort study. Pharmacoepidemiol Drug Saf. 2011; 20:111–118. [PubMed: 21254281]
16. Spiro AS, Beil FT, Schinke T, et al. Short-term application of dexamethasone enhances bone morphogenetic protein-7-induced ectopic bone formation in vivo. J Trauma. 2010; 69:1473–1480. [PubMed: 21150526]
17. Spiro AS, Beil FT, Baranowsky A, et al. BMP-7-induced ectopic bone formation and fracture healing is impaired by systemic NSAID application in C57BL/6-mice. J Orthop Res. 2010; 28:785–791. [PubMed: 20063306]
18. Giannoudis PV, Jones E, Einhorn TA. Fracture healing and bone repair. Injury. 2011; 42:549–550. [PubMed: 21474131]
19. Hadjiargyrou M, O'keefe RJ. The convergence of fracture repair and stem cells: Inter-play of genes, aging, environmental factors and disease. J Bone Miner Res. 2014; 29:2307–2322. [PubMed: 25264148]

20. Gomez-Barrena E, Rosset P, Lozano D, et al. Bone fracture healing: Cell therapy in delayed unions and nonunions. Bone. 2015; 70:93–101. [PubMed: 25093266]
21. Kawano S, Otsu K, Kuruma A, et al. ATP autocrine/paracrine signaling induces calcium oscillations and NFAT activation in human mesenchymal stem cells. Cell Calcium. 2006; 39:313–324. [PubMed: 16445977]
22. Mayer H, Bertram H, Lindenmaier W, et al. Vascular endothelial growth factor (VEGF-a) expression in human mesenchymal stem cells: Autocrine and paracrine role on osteoblastic and endothelial differentiation. J Cell Biochem. 2005; 95:827–839. [PubMed: 15838884]
23. Kim J, Ma T. Autocrine fibroblast growth factor 2-mediated interactions between human mesenchymal stem cells and the extracellular matrix under varying oxygen tension. J Cell Biochem. 2013; 114:716–727. [PubMed: 23060043]
24. Briolay A, Lencel P, Bessueille L, et al. Autocrine stimulation of osteoblast activity by Wnt5a in response to TNF-alpha in human mesenchymal stem cells. Biochem Biophys Res Commun. 2013; 430:1072–1077. [PubMed: 23266365]
25. Bastiaans J, van Meurs JC, van Holten-Neelen C, et al. Thrombin induces epithelial-mesenchymal transition and collagen production by retinal pigment epithelial cells via autocrine PDGF-receptor signaling. Invest Ophthalmol Vis Sci. 2013; 54:8306–8314. [PubMed: 24302586]
26. Alcaraz A, Mrowiec A, Insausti CL, et al. Autocrine TGF-beta induces epithelial to mesenchymal transition in human amniotic epithelial cells. Cell Transplant. 2013; 22:1351–1367. [PubMed: 23031712]
27. Fruscione F, Scarfi S, Ferraris C, et al. Regulation of human mesenchymal stem cell functions by an autocrine loop involving NAD1 release and P2Y11-mediated signaling. Stem Cells Dev. 2011; 20:1183–1198. [PubMed: 20964598]
28. Yao W, Guan M, Jia J, et al. Reversing bone loss by directing mesenchymal stem cells to the Bone. Stem Cells. 2013
29. Guan M, Yao W, Liu R, et al. Directing mesenchymal stem cells to bone to augment bone formation and increase bone mass. Nat Med. 2012; 18:456–462. [PubMed: 22306732]
30. Chokalingam K, Roforth MM, Nicks KM, et al. Examination of ERalpha signaling pathways in bone of mutant mouse models reveals the importance of ERE-dependent signaling. Endocrinology. 2012; 153:5325–5333. [PubMed: 23015293]
31. Beck TJ, Ruff CB, Shaffer RA, et al. Stress fracture in military recruits: Gender differences in muscle and bone susceptibility factors. Bone. 2000; 27:437–444. [PubMed: 10962357]
32. Gao X, Usas A, Proto JD, et al. Role of donor and host cells in muscle-derived stem cell-mediated bone repair: differentiation vs. paracrine effects. FASEB J. 2014; 28:3792–3809. [PubMed: 24843069]
33. Deasy BM, Schugar RC, Huard J. Sex differences in muscle-derived stem cells and skeletal muscle. Crit Revi Eukaryot Gene Expr. 2008; 18:173–188.
34. Meszaros LB, Usas A, Cooper GM, et al. Effect of host sex and sex hormones on muscle-derived stem cell-mediated bone formation and defect healing. Tissue Eng Part A. 2012; 18:1751–1759. [PubMed: 22712541]
35. Katsara O, Mahaira LG, Iliopoulou EG, et al. Effects of donor age, gender, and in vitro cellular aging on the phenotypic, functional, and molecular characteristics of mouse bone Marrow-derived mesenchymal stem Cells. Stem Cells Dev. 2011
36. Crisostomo PR, Wang M, Herring CM, et al. Gender differences in injury induced mesenchymal stem cell apoptosis and VEGF, TNF, IL-6 expression: Role of the 55 kDa TNF receptor (TNFR1). J Mol Cell Cardiol. 2007; 42:142–149. [PubMed: 17070836]
37. Matsumoto T, Kubo S, Meszaros LB, et al. The influence of sex on the chondrogenic potential of muscle-derived stem cells: Implications for cartilage regeneration and repair. Arthritis Rheum. 2008; 58:3809–3819. [PubMed: 19035511]
38. Corsi KA, Pollett JB, Phillippi JA, et al. Osteogenic potential of postnatal skeletal muscle-derived stem cells is influenced by donor sex. J Bone Miner Res. 2007; 22:1592–1602. [PubMed: 17605633]

39. Ota S, Uehara K, Nozaki M, et al. Intra-muscular transplantation of muscle-derived stem cells accelerates skeletal muscle healing after contusion injury via enhancement of angiogenesis. Am J Sports Med. 2011; 39:1912–1922. [PubMed: 21828363]
40. Deasy BM, Lu A, Tebbets JC, et al. A role for cell sex in stem cell-mediated skeletal muscle regeneration: Female cells have higher muscle regeneration efficiency. J Cell Biol. 2007; 177:73–86. [PubMed: 17420291]
41. Kitaori T, Ito H, Schwarz EM, et al. Stromal cell-derived factor 1/CXCR4 signaling is critical for the recruitment of mesenchymal stem cells to the fracture site during skeletal repair in a mouse model. Arthritis Rheum. 2009; 60:813–823. [PubMed: 19248097]
42. Granero-Molto F, Weis JA, Miga MI, et al. Regenerative effects of transplanted mesenchymal stem cells in fracture healing. Stem Cells. 2009; 27:1887–1898. [PubMed: 19544445]
43. Granero-Molto F, Myers TJ, Weis JA, et al. Mesenchymal stem cells expressing insulin-like growth factor-I (MSCIGF) promote fracture healing and restore new bone formation in Irs1 knockout mice: Analyses of MSCIGF autocrine and paracrine regenerative effects. Stem Cells. 2011; 29:1537–1548. [PubMed: 21786367]
44. Dreger T, Watson JT, Akers W, et al. Intravenous application of CD271-selected mesenchymal stem cells during fracture healing. J Orthop Trauma. 2014; 28:S15–S19.
45. Colnot C, Huang S, Helms J. Analyzing the cellular contribution of bone marrow to fracture healing using bone marrow transplantation in mice. Biochem Biophys Res Commun. 2006; 350:557–561. [PubMed: 17022937]
46. Manigrasso MB, O'connor JP. Characterization of a closed femur fracture model in mice. J Orthop Trauma. 2004; 18:687–695. [PubMed: 15507822]
47. Holstein JH, Matthys R, Histing T, et al. Development of a stable closed femoral fracture model in mice. J Surg Res. 2009; 153:71–75. [PubMed: 18656902]
48. Nishimura R, Wakabayashi M, Hata K, et al. Osterix regulates calcification and degradation of chondrogenic matrices through matrix metalloproteinase 13 (MMP13) expression in association with transcription factor Runx2 during endochondral ossification. J Biol Chem. 2012; 287:33179–33190. [PubMed: 22869368]
49. Mizoguchi T, Pinho S, Ahmed J, et al. Osterix marks distinct waves of primitive and definitive stromal progenitors during bone marrow development. Dev Cell. 2014; 29:340–349. [PubMed: 24823377]
50. Liu Y, Strecker S, Wang L, et al. Osterix-cre labeled progenitor cells contribute to the formation and maintenance of the bone marrow stroma. PLoS One. 2013; 8:e71318. [PubMed: 23951132]
51. Freeman TA, Patel P, Parvizi J, et al. Micro-CT analysis with multiple thresholds allows detection of bone formation and resorption during ultrasound-treated fracture healing. J Orthop Res. 2009; 27:673–679. [PubMed: 19016539]
52. Yao W, Dai W, Shahnazari M, et al. Inhibition of the progesterone nuclear receptor during the bone linear growth phase increases peak bone mass in female mice. PLoS One. 2010; 5:e11410. [PubMed: 20625385]
53. Yao W, Cheng Z, Shahnazari M, et al. Overexpression of secreted frizzled-related protein 1 inhibits bone formation and attenuates parathyroid hormone bone anabolic effects. J Bone Miner Res. 2010; 25:190–199. [PubMed: 19594295]
54. Yao W, Cheng Z, Pham A, et al. Glucocorticoid-induced bone loss in mice can be reversed by the actions of parathyroid hormone and risedronate on different pathways for bone formation and mineralization. Arthritis Rheum. 2008; 58:3485–3497. [PubMed: 18975341]
55. Dempster DW, Compston JE, Drezner MK, et al. Standardized nomenclature, symbols, and units for bone histomorphometry: A 2012 update of the report of the ASBMR histomorphometry nomenclature Committee. J Bone Miner Res. 2013; 28:2–17. [PubMed: 23197339]
56. Parfitt AM, Drezner MK, Glorieux FH, et al. Bone histomorphometry: Standardization of nomenclature, symbols, and units. Report of the ASBMR Histomorphometry Nomenclature Committee. J Bone Miner Res. 1987; 2:595–610. [PubMed: 3455637]
57. Lane NE, Yao W, Balooch M, et al. Gluco-corticoid-treated mice have localized changes in trabecular bone material properties and osteocyte lacunar size that are not observed in placebo-treated or estrogen-deficient mice. J Bone Miner Res. 2006; 21:466–476. [PubMed: 16491295]

58. Lane NE, Yao W, Nakamura MC, et al. Mice lacking the integrin beta5 subunit have accelerated osteoclast maturation and increased activity in the estrogen-deficient state. J Bone Miner Res. 2005; 20:58–66. [PubMed: 15619670]
59. Yao W, Cheng Z, Koester KJ, et al. The degree of bone mineralization is maintained with single intravenous bisphosphonates in aged estrogen-deficient rats and is a strong predictor of bone strength. Bone. 2007; 41:804–812. [PubMed: 17825637]
60. Balooch G, Yao W, Ager JW, et al. The aminobisphosphonate risedronate preserves localized mineral and material properties of bone in the presence of glucocorticoids. Arthritis Rheum. 2007; 56:3726–3737. [PubMed: 17968931]
61. Turner CH, Burr DB. Basic biomechanical measurements of bone: A tutorial. Bone. 1993; 14:595–608. [PubMed: 8274302]
62. Grcevic D, Pejda S, Matthews BG, et al. In vivo fate mapping identifies mesenchymal progenitor Cells. Stem Cells. 2012; 30:187–196. [PubMed: 22083974]
63. Matthews BG, Grcevic D, Wang L, et al. Analysis of alphaSMA-labeled progenitor cell commitment identifies notch signaling as an important pathway in fracture healing. J Bone Miner Res. 2014; 29:1283–1294. [PubMed: 24190076]
64. Turner CH. Bone strength: Current concepts. Ann NY Acad Sci. 2006; 1068:429–446. [PubMed: 16831941]
65. Chapel A, Bertho JM, Bensidhoum M, et al. Mesenchymal stem cells home to injured tissues when co-infused with hematopoietic cells to treat a radiation-induced multi-organ failure syndrome. J Gene Med. 2003; 5:1028–1038. [PubMed: 14661178]
66. Huang S, Xu L, Zhang Y, et al. Systemic and local administration of allogeneic bone Marrow-derived mesenchymal stem cells promotes fracture healing in rats. Cell Transplant. 2015; 24:2643–2655. [PubMed: 25647659]
67. Vogel S, Borger V, Peters C, et al. Necrotic cell-derived high mobility group box 1 attracts antigen-presenting cells but inhibits hepatocyte growth factor-mediated tropism of mesenchymal stem cells for apoptotic cell death. Cell Death Differ. 2015; 22:1219–1230. [PubMed: 25571972]
68. Miedel E, Dishowitz MI, Myers MH, et al. Disruption of thrombospondin-2 accelerates ischemic fracture healing. J Orthop Res. 2013; 31:935–943. [PubMed: 23280580]
69. Taylor DK, Meganck JA, Terkhorn S, et al. Thrombospondin-2 influences the proportion of cartilage and bone during fracture healing. J Bone Miner Res. 2009; 24:1043–1054. [PubMed: 19123916]
70. Miles LA, Plow EF, Waisman DM, et al. Plasminogen receptors. J Biomed Biotechnol. 2012; 2012:130735. [PubMed: 23226936]
71. Copland IB, Lord-Dufour S, Cuerquis J, et al. Improved autograft survival of mesenchymal stromal cells by plasminogen activator inhibitor 1 inhibition. Stem Cells. 2009; 27:467–477. [PubMed: 19338064]
72. Kisiday JD, Hale BW, Almodovar JL, et al. Expansion of mesenchymal stem cells on fibrinogen-rich protein surfaces derived from blood plasma. J Tissue Eng Regen Med. 2011; 5:600–611. [PubMed: 21774083]
73. Linsley C, Wu B, Tawil B. The effect of fibrinogen, collagen type I, and fibronectin on mesenchymal stem cell growth and differentiation into osteoblasts. Tissue Eng Part A. 2013; 19:1416–1423. [PubMed: 23360404]
74. Bahney CS, Hsu CW, Yoo JU, et al. A bio-responsive hydrogel tuned to chondrogenesis of human mesenchymal stem cells. FASEB J. 2011; 25:1486–1496. [PubMed: 21282205]
75. Djouad F, Delorme B, Maurice M, et al. Microenvironmental changes during differentiation of mesenchymal stem cells towards chondrocytes. Arthritis Res Ther. 2007; 9:R33. [PubMed: 17391539]
76. English K, Ryan JM, Tobin L, et al. Cell contact, prostaglandin E(2) and transforming growth factor beta 1 play non-redundant roles in human mesenchymal stem cell induction of CD41CD25(High) forkhead box P31 regulatory T cells. Clin Exp Immunol. 2009; 156:149–160. [PubMed: 19210524]

77. Hermankova B, Zajicova A, Javorkova E, et al. Suppression of IL-10 production by activated B cells via a cell contact-dependent cyclooxygenase-2 pathway upregulated in IFN-gamma-treated mesenchymal stem cells. Immunobiology. 2015
78. Hajkova M, Javorkova E, Zajicova A, et al. A local application of mesenchymal stem cells and cyclosporine a attenuates immune response by a switch in macrophage phenotype. J Tissue Eng Regen Med. 2015
79. Polchert D, Sobinsky J, Douglas G, et al. IFN-gamma activation of mesenchymal stem cells for treatment and prevention of graft versus host disease. Eur J Immunol. 2008; 38:1745–1755. [PubMed: 18493986]
80. Sivanathan KN, Gronthos S, Rojas-Canales D, et al. Interferon-gamma modification of mesenchymal stem cells: Implications of autologous and allogeneic mesenchymal stem cell therapy in allotransplantation. Stem Cell Rev. 2014; 10:351–375. [PubMed: 24510581]
81. Bernardo ME, Fibbe WE. Mesenchymal stromal cells: Sensors and switchers of inflammation. Cell Stem Cell. 2013; 13:392–402. [PubMed: 24094322]
82. Zhang QZ, Su WR, Shi SH, et al. Human gingiva-derived mesenchymal stem cells elicit polarization of m2 macrophages and enhance cutaneous wound healing. Stem Cells. 2010; 28:1856–1868. [PubMed: 20734355]
83. Melief SM, Schrama E, Brugman MH, et al. Multipotent stromal cells induce human regulatory T cells through a novel pathway involving skewing of monocytes toward anti-inflammatory macrophages. Stem Cells. 2013; 31:1980–1991. [PubMed: 23712682]
84. Lohan P, Coleman CM, Murphy JM, et al. Changes in immunological profile of allogeneic mesenchymal stem cells after differentiation: Should we be concerned? Stem Cell Res Ther. 2014; 5:99. [PubMed: 25158057]
85. Zanier ER, Pischiutta F, Riganti L, et al. Bone marrow mesenchymal stromal cells drive protective M2 microglia polarization after brain trauma. Neurotherapeutics. 2014; 11:679–695. [PubMed: 24965140]
86. Cho DI, Kim MR, Jeong HY, et al. Mesenchymal stem cells reciprocally regulate the M1/M2 balance in mouse bone marrow-derived macrophages. Exp Mol Med. 2014; 46:e70. [PubMed: 24406319]
87. Sheyn D, Shapiro G, Tawackoli W, et al. PTH induces systemically administered mesenchymal stem cells to migrate to and regenerate spine Injuries. Mol Ther. 2015
88. Ominsky MS, Li C, Li X, et al. Inhibition of sclerostin by monoclonal antibody enhances bone healing and improves bone density and strength of nonfractured bones. J Bone Miner Res. 2011; 26:1012–1021. [PubMed: 21542004]
89. Einhorn TA. Can an anti-fracture agent heal fractures? Clin Cases Miner Bone Metab. 2010; 7:11–14. [PubMed: 22461283]
90. Peter CP, Cook WO, Nunamaker DM, et al. Effect of alendronate on fracture healing and bone remodeling in dogs. J Orthop Res. 1996; 14:74–79. [PubMed: 8618170]
91. Li C, Mori S, Li J, et al. Long-term effect of incadronate disodium (YM-175) on fracture healing of femoral shaft in growing rats. J Bone Miner Res. 2001; 16:429–436. [PubMed: 11277259]

Significance Statement

The current study used a clinically relevant preclinical fracture model of both sexes and found that treatment with a novel hybrid compound, LLP2A-Ale, that mobilizes endogenous MSCs to bone remodeling sites, with transplanted MSCs, increaesd engraftment of MSCs to the fracture site. This was associated with augmented bone formation that resulted in improved bone strength. In addition, we found that increased mobilization of exogenous MSCs to facture sites accelerated endochondral bone formation partially through paracrine signaling to enhance bone tissue regeneration. These results are important for targeted delivery of MSCs for fracture repair through direct cell differentiation and paracrine mechanisms.

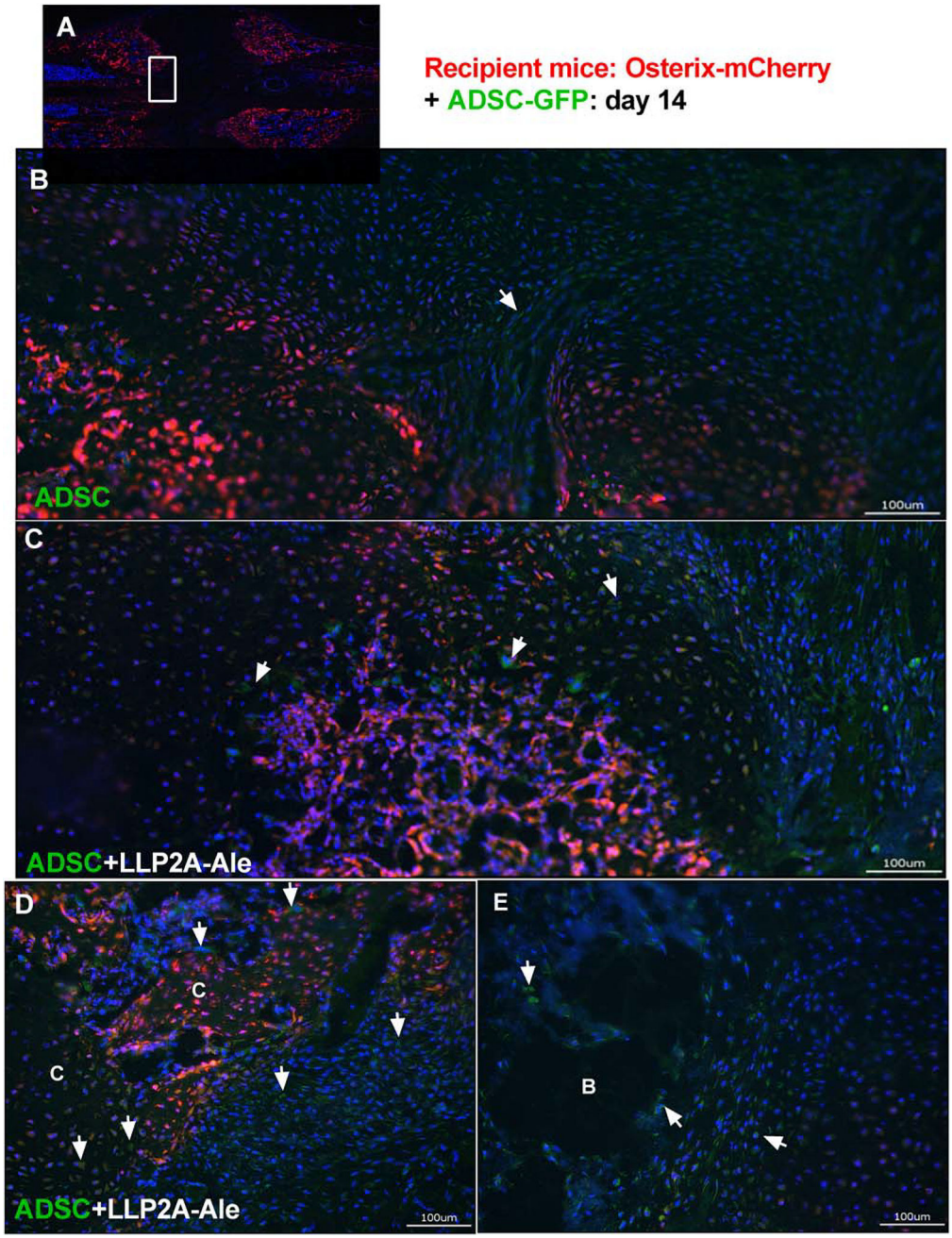

Figure 1.

LLP2A-Ale increased mobilization of exogenous mesenchymal stem cells (MSCs) to fracture gaps at day 14. Femurs of Osterix-mCherry reporter mice were fractured at two-months of age and these animals received 5×10^5 ADSC-GFP or ADSC + LLP2A-Ale IV on the day of fracture. Mice were euthanized 14 days postfracture. Images were taken at the center of the fracture gaps from representative female mice (**A**) that received ADSC (**B**) or ADSC + LLP2A-Ale (**C–E**). White arrows illustrate ADSC-GFP cells that were mobilized to the fracture gaps or adjacent to the dead bone fragments. Abbreviations: ADSC, adipose-

derived MSC; B, bone fragment C, callus; GFP, green-florescence protein; LLP2A-Ale, LLP2A-Alendronate. Scale bar: 100μm.

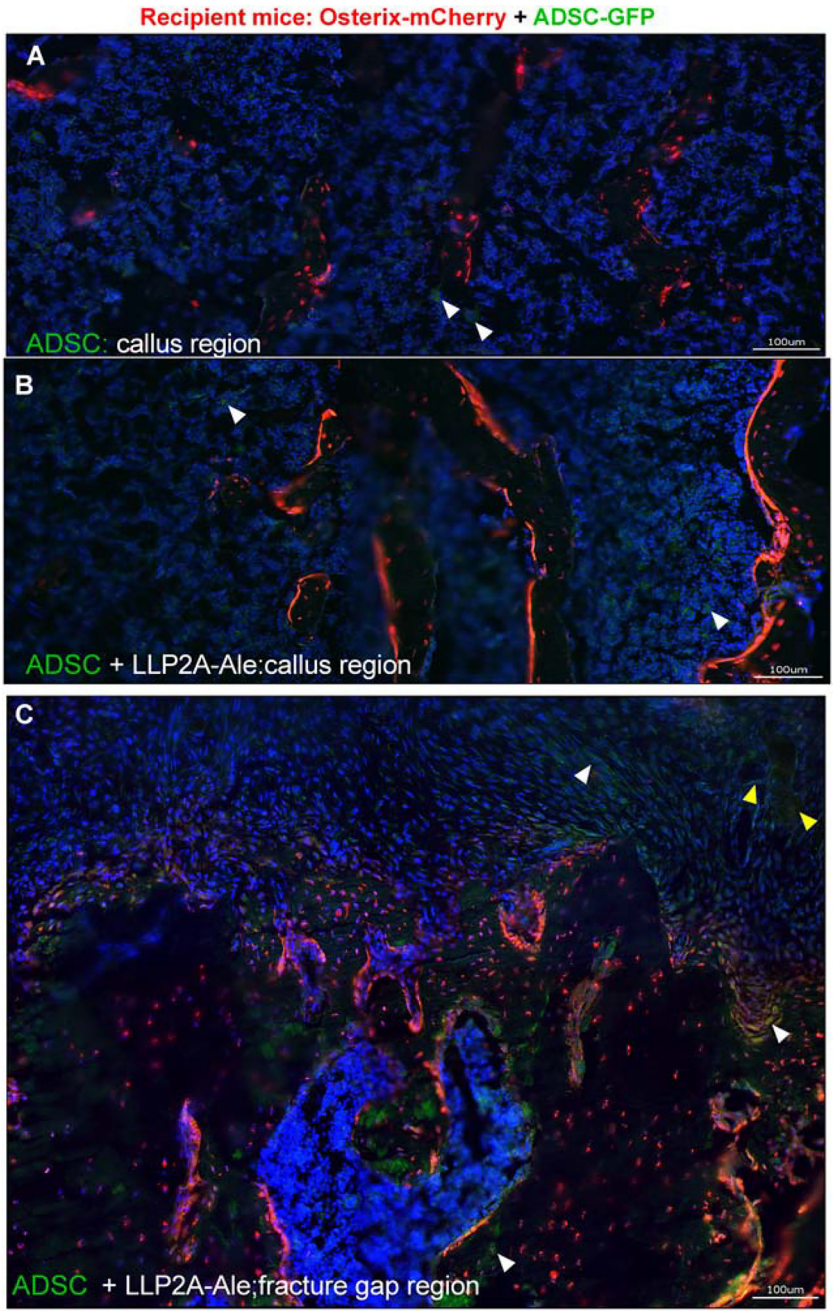

Figure 2.

LLP2A-Ale enhanced the engraftment of mesenchymal stem cell (MSCs) and contributed to endochondral bone formation at day 21. Femurs of Osterix-mCherry reporter mice were fractured at two-months of age, and these animals received 5×10^5 ADSC-GFP or ADSC + LLP2A-Ale IV on the day of fracture. Mice were euthanized 21 days postfracture. Images were taken at the center of the callus similar to the region demonstrated in Figure 1A. Representative images were taken from male mice (**A**) that received ADSC or ADSC + LLP2A-Ale (**B** and **C**). White arrow-heads illustrate ADSC-GFP cells that were detected in the bone marrow within the callus. Some of the GFP+ cells were seen incorporated into the

callus or embedded in the mineralization front, forming bone-like foci (yellow arrow heads). Scale bar: 100 μm. Abbreviations: ADSC, adipose-derived MSC; GFP, green-florescence protein; LLP2A-Ale, LLP2A-Alendronate.

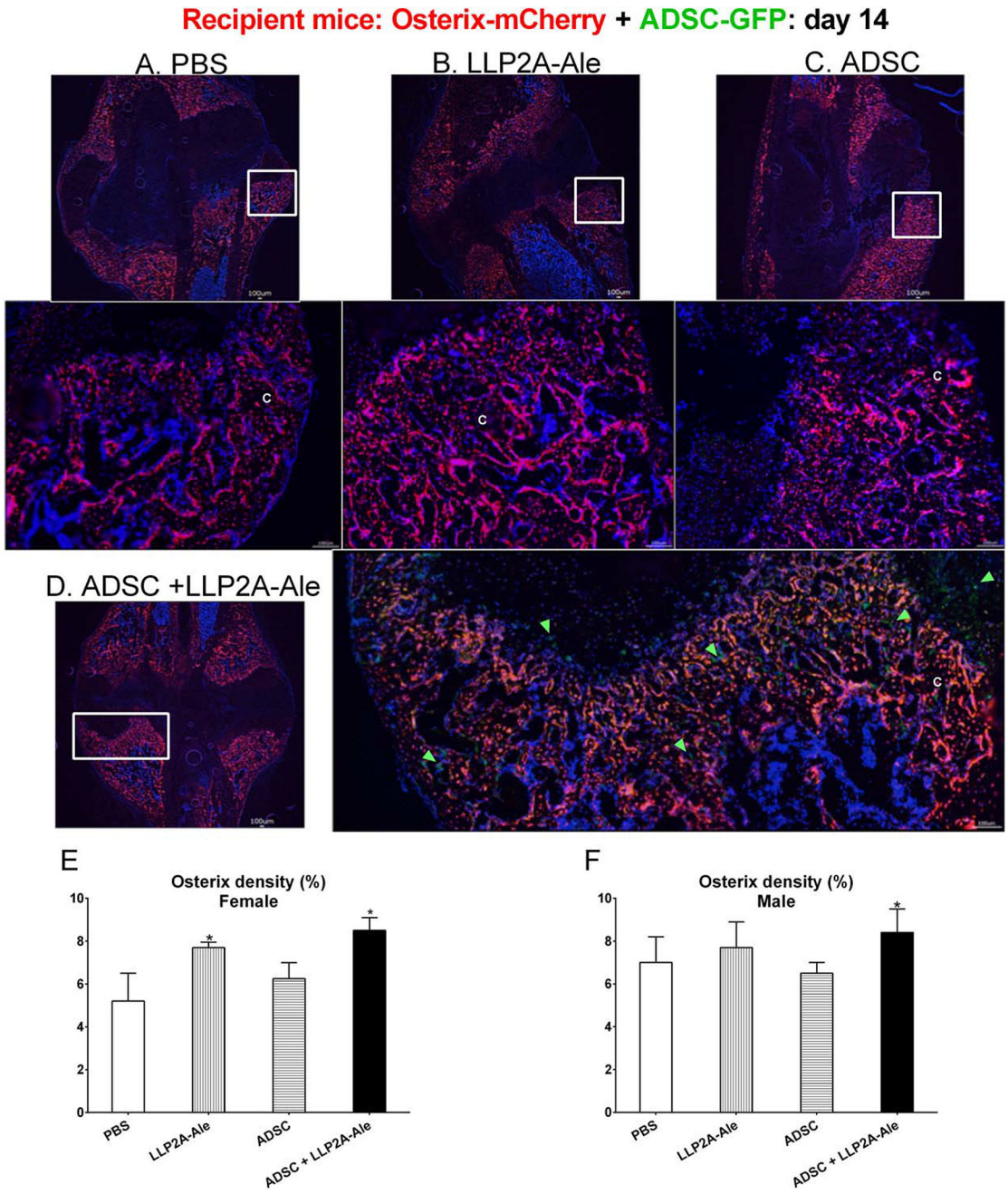

Figure 3.

Effects of LLP2A-Ale or combination treatment with ADSC on endogenous osteogenesis. Femurs of Osterix-mCherry reporter mice were fractured at two-months of age, and these animals received PBS (**A**), LLP2A-Ale (**B**), ADSC-GFP (**C**), or ADSC + LLP2A-Ale (**D**). Mice were euthanized 14 days post-fracture. Green arrows illustrated ADSC-GFP cells that were detected within the fracture gaps and embedded in the callus in the ADSC + LLP2A-Ale group (D). Density of osterix expression was calculated for the entire callus region for recipients from both sexes (**E** and **F**). Representative images were taken from male mice as indicated in white squares. *, $p < .05$ versus PBS-treated group. Scale bar: 100 μm.

Abbreviations: ADSC, adipose-derived MSC; GFP, green-flourescence protein; LLP2A-Ale, LLP2A-Alendronate; PBS, phosphate buffered saline.

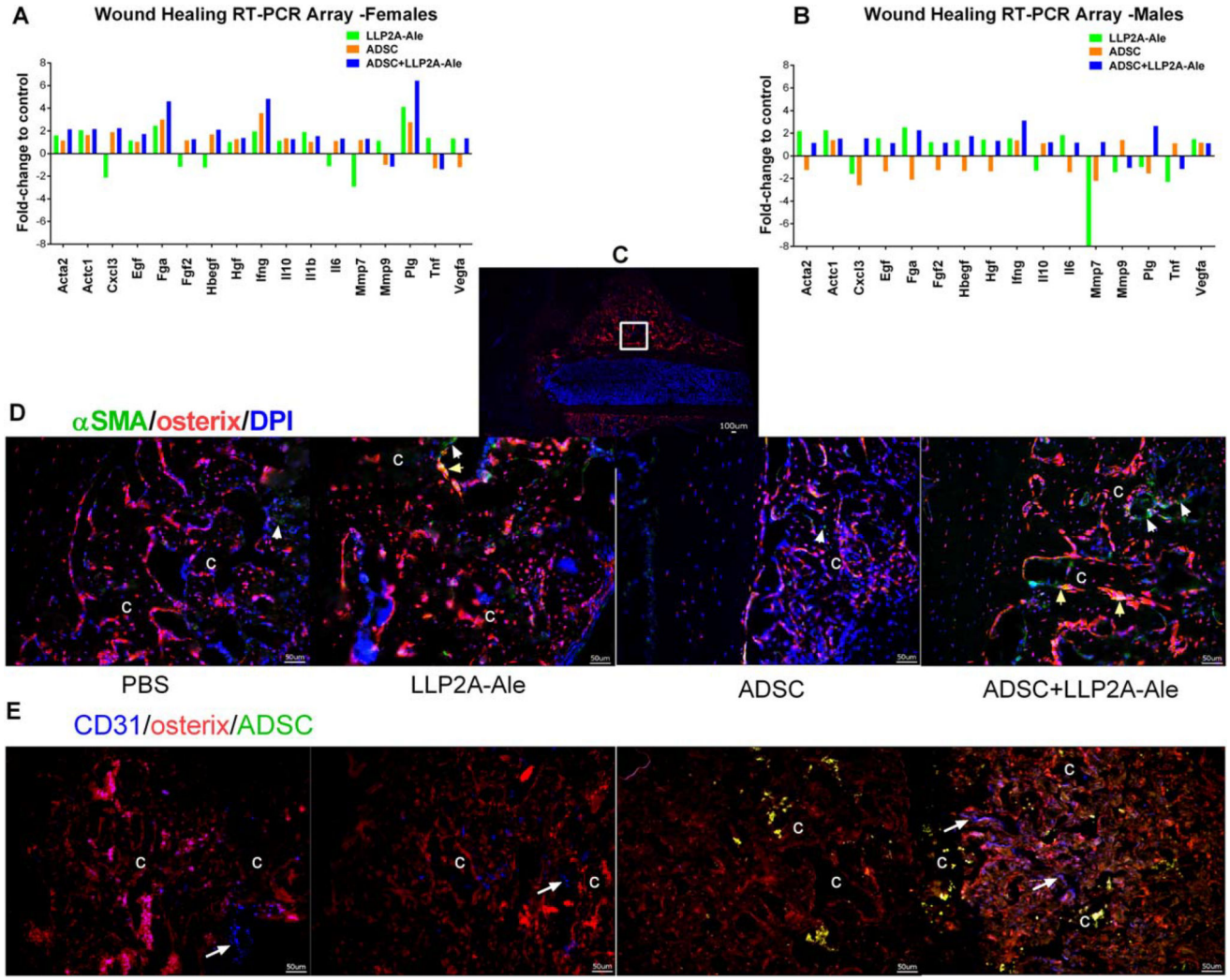

Figure 4.

LLP2A-Ale and ADSC had synergistic effects on wound healing. Femurs of Osterix-mCherry reporter mice were fractured at two-months of age, and these animals received 5×10^5 ADSC or ADSC + LLP2A-Ale IV on the day of fracture. Mice were euthanized 14 days post-fracture. RNA was extracted from calluses and used for RT-PCR gene arrays focused on wound healing. Genes that differed significantly from PBS-treated mice are shown for females (**A**) and males (**B**). Immunohistochemistry was used to confirm αSMA (**D**) and angiogenesis (anti-CD31) (**E**) in male Osx-mCherry mice that received ADSC without (green-florescence protein) GFP transfection. White arrows indicate αSMA+ cells at the callus (green fluorescence), and yellow arrows indicate αSMA+ that differentiated into osteoblasts (yellow fluorescence). Angiogenesis was marked by anti-CD31 staining (white long arrows, blue fluorescence). Scale bar: 100 μm. Abbreviations: ADSC, adipose-derived MSC; LLP2A-Ale, LLP2A-Alendronate.

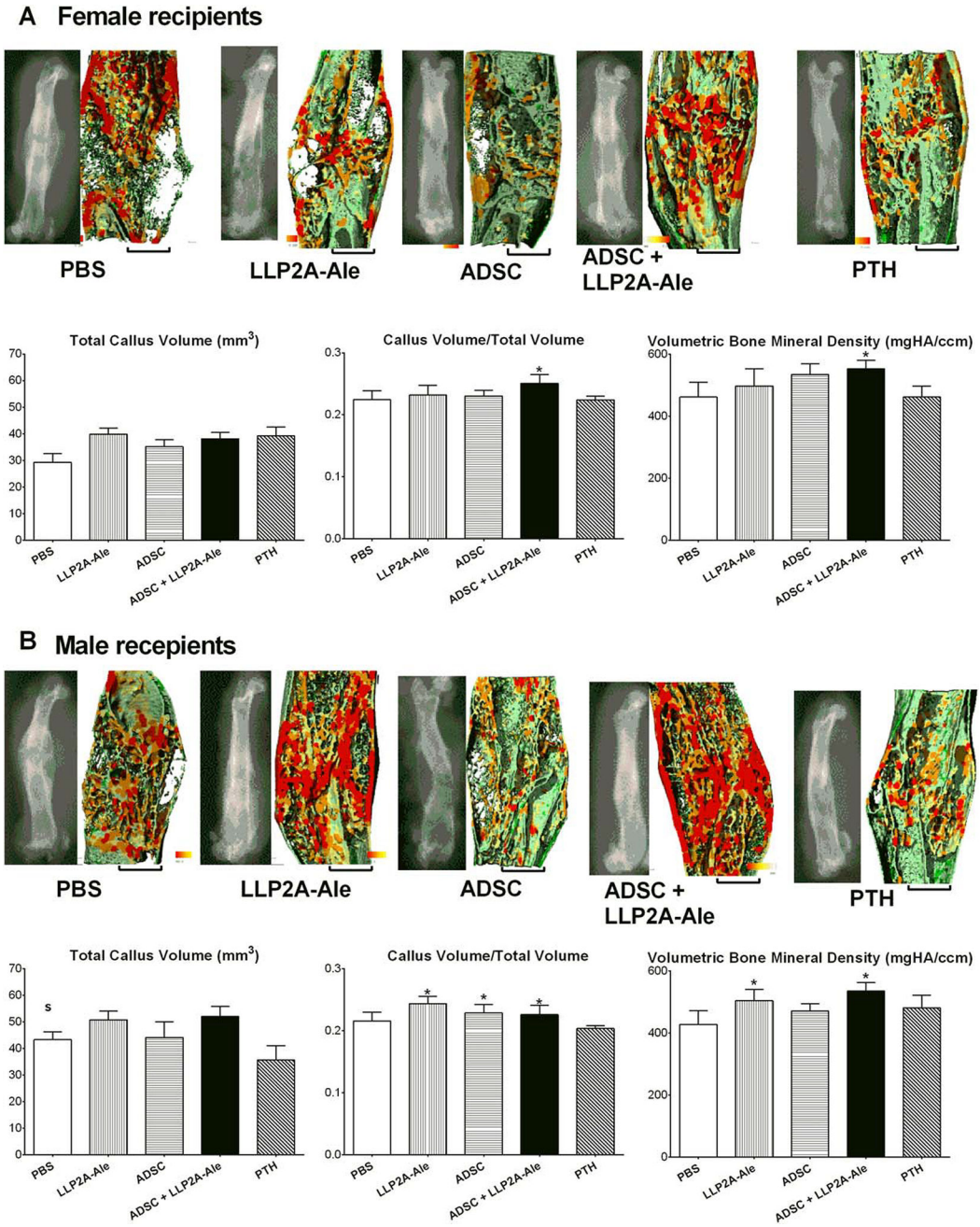

Figure 5.

ADSC and LLP2A-Ale cotreatment induced higher callus bone volume and volumetric bone mineral density (vBMD) at day 42. MicroCT measurements were performed at day 42 for all treatment groups. Total callus volume, callus volume fraction, vBMD and representative lateral views of 2D and 3D reconstructions of microCT thickness mappings are shown for both females (**A**) and males (**B**). MicroCT thickness images were color-coded for trabecular thickness, where thicker trabeculae are shown in red and thinner ones are shown in green. *, $p < .05$ versus PBS-treated group; ^{S}, $p < .05$ versus females. Scale bar: 1.0 mm.

Abbreviations: ADSC, adipose-derived MSC; LLP2A-Ale, LLP2A-Alendronate; PBS, phosphate buffered saline; PTH, parathyroid hormone.

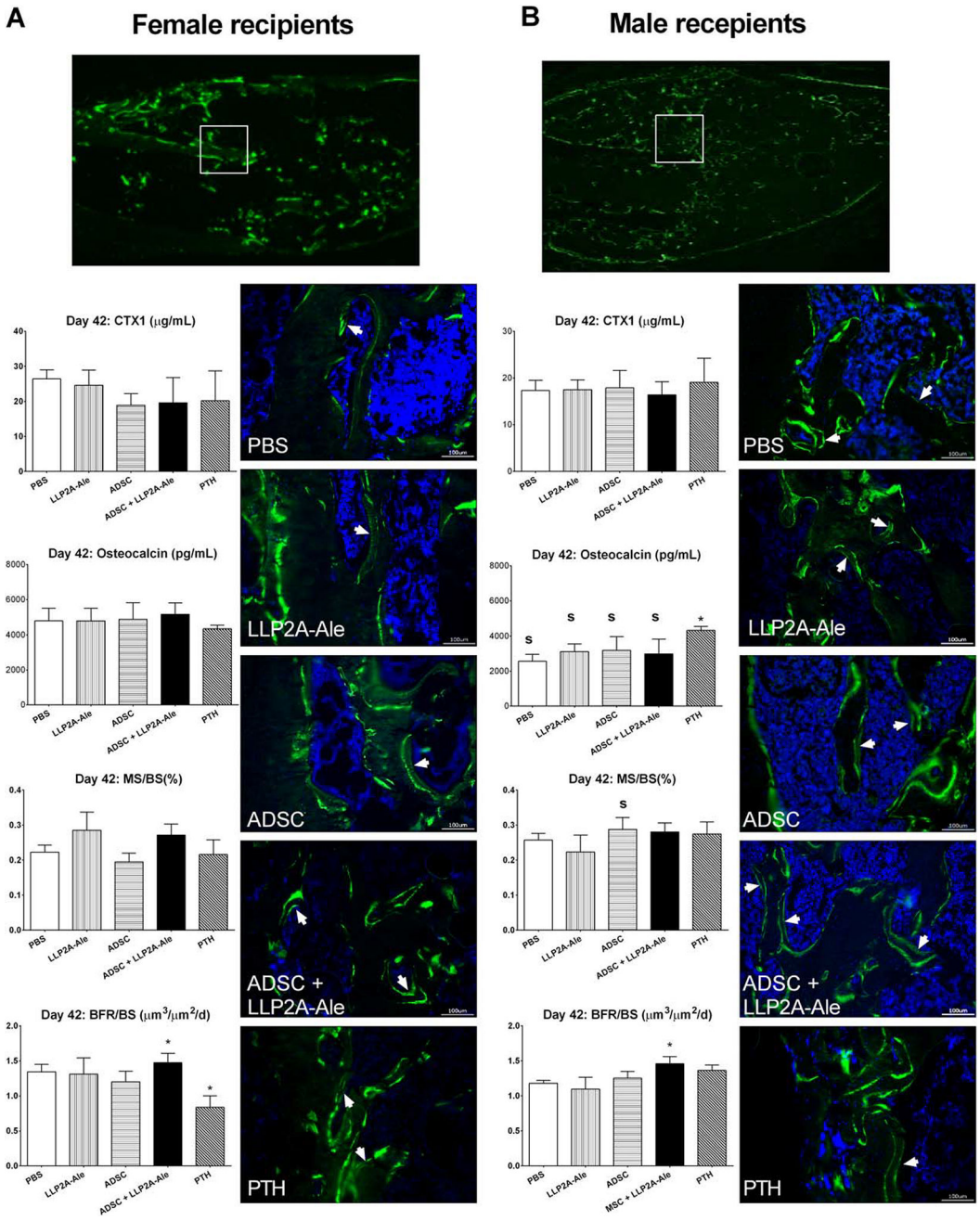

Figure 6.

ADSC and LLP2A-Ale cotreatment induced higher callus mineralization and bone formation. Double-calcein-labeled histologic sections were obtained from both female (**A**) and male mice (**B**). White boxes indicated the approximate position of the enlarged representative fluorescent images taken from various treatment groups. White arrows indicate double-labeled callus surfaces that were undergoing active bone mineralization. *, $p < .05$ versus PBS-treated group; ^{S}, $p < .05$ versus females. Scale bar: 100 μm. Abbreviations: ADSC, adipose-derived MSC; BFR/BS, surface-based bone formation rate; LLP2A-Ale,

LLP2A-Alendronate; MS/BS, mineralized bone surface; PBS, phosphate buffered saline; PTH, parathyroid hormone.

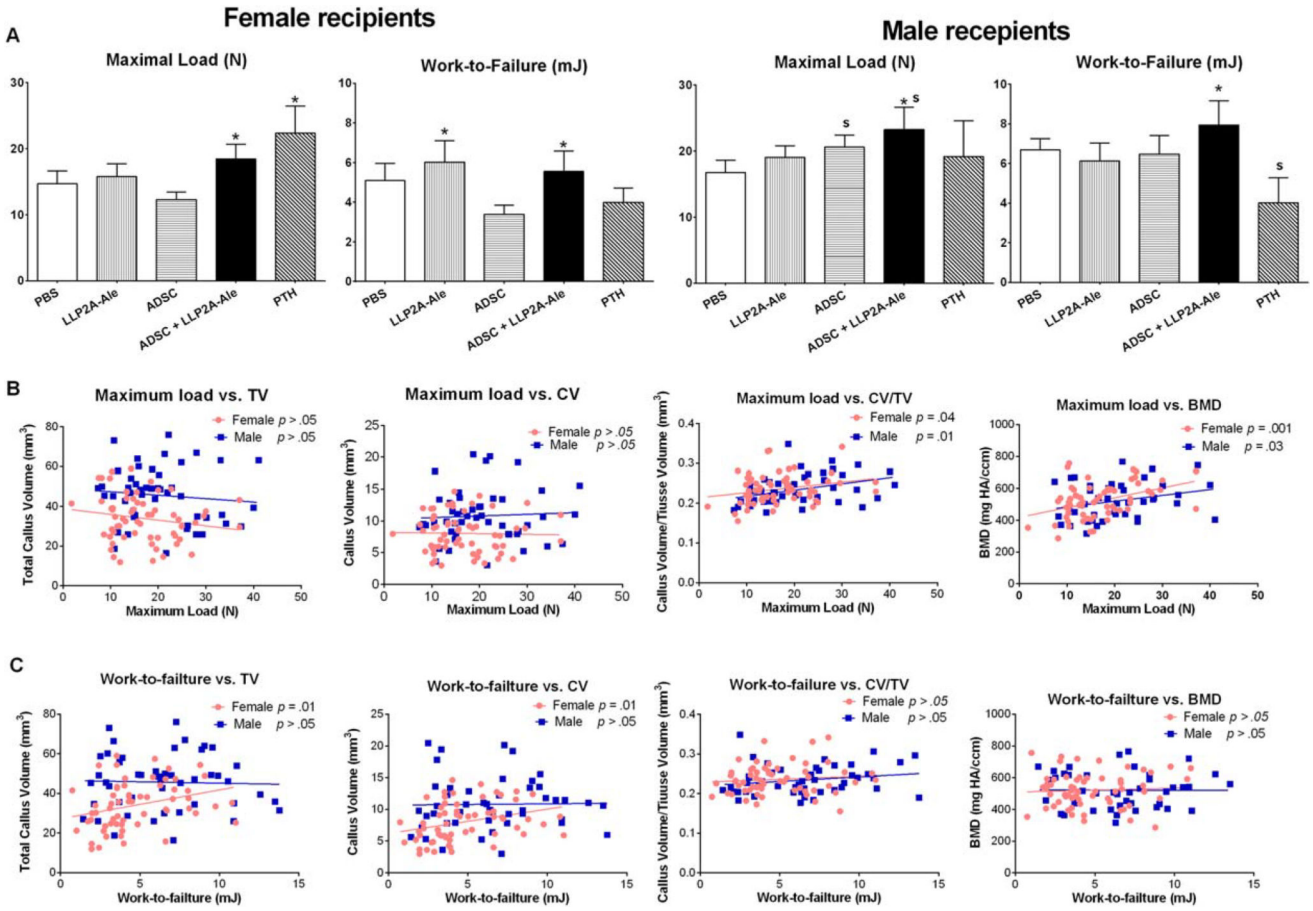

Figure 7.

ADSC and LLP2A-Ale cotreatment increased bone strength. Four-point bending was performed to obtain maximum load and to calculate work-to-failure for all of the treatment groups at day 42 (**A**). Linear regression was performed for callus structural parameters versus maximum load (**B**) or work-to-failure (**C**) and separated for females and the males. *, $p < .05$ versus PBS-treated group; ^{S}, $p < .05$ versus females. Abbreviations: ADSC, adipose-derived MSC; CV, callus new bone volume; CV/TV, callus volume fraction; LLP2A-Ale, LLP2A-Alendronate; PBS, phosphate buffered saline; PTH, parathyroid hormone; TV, total callus volume; BMD, bone mineral density.